Photophysical Properties of Homometallic Ruthenium(II) and Osmium(II) Complexes with a Bis(dipyridophenazine) Bridging Ligand. From Pico- to Microsecond Time Resolution

Mara Staffilani,[†] Peter Belser,[‡] František Hartl,[†] Cornelis J. Kleverlaan,[†] and Luisa De Cola*[,†]

Institute of Molecular Chemistry, Molecular Photonic Materials, Universiteit van Amsterdam, Nieuwe Achtergracht 166, 1018 WV Amsterdam, The Netherlands, and Institute of Inorganic and Analytical Chemistry, University of Fribourg, Pérolles, 1700 Fribourg, Switzerland

Received: April 24, 2002; In Final Form: July 18, 2002

The photophysical properties of [Ru-bidppz-Ru]$^{4+}$, [Os-bidppz-Os]$^{4+}$, and the bridging ligand bidppz (bidppz = 1,1′-dipyrido[3,2-*a*:2′,3′-*c*]phenazin-1,1′-yldipyrido[3,2-*a*:2′,3′-*c*]phenazine) are investigated. Time-resolved spectroscopic studies were performed on (sub)pico- to microsecond time scales, offering insight into the excited states responsible for the photophysical behavior of the two complexes in different solvents. In particular, [Ru-bidppz-Ru]$^{4+}$ shows a long excited-state lifetime, 9.7 μs, in deaerated dichloromethane solution, that becomes much shorter (360 ns) in deaerated butyronitrile. The solvent plays a crucial role for the spectroscopic properties of this complex, since the energy of the triplet metal-to-ligand charge-transfer (^{3}MLCT) excited state is influenced by the polarity of the medium. (Sub)picosecond transient absorption spectra in dichloromethane indicate thermal population of the long-lived triplet intraligand (^{3}IL) state of the bridging ligand from the lower lying ^{3}MLCT state. For [Os-bidppz-Os]$^{4+}$ in dichloromethane the ^{3}MLCT state lies lower in energy and no interaction of this state with the ^{3}IL state of the bridging ligand is observed.

Introduction

Transition metal complexes and in particular ruthenium compounds exhibiting long-lived luminescent excited state are extensively studied for their potential application in diverse areas such as luminescence sensing,[1−3] DNA probes,[4,5] and medical diagnostics.[6,7] The increase of the excited-state lifetime can be achieved by electronic and structural control of the coordinating ligands. Ligand delocalization and rigidity increase the excited-state lifetime but often decrease the energy gap between the excited and ground state.[8,9] The presence of a low-lying ligand-localized triplet state, which can strongly interact with a metal-to-ligand charge-transfer (MLCT) excited state of the ruthenium moiety, has received a lot of attention, for instance in Ru(II)−pyrene complexes[10−16] and in solvatochromic aromatic systems appended to a ruthenium unit.[17] Such an approach has the advantage that the system can be designed according to the energy levels of the ruthenium moiety and the appended ligand.

In some cases attempts to build up large aromatic ligands containing the chelating site were also successful.[8]

Among the flat aromatic ligands that can influence the spectroscopic properties of the ruthenium moiety, the most studied has been the well-known dppz (dppz = dipyrido[3,2-*a*:2′,3′-*c*]phenazine), and its metal complexes have been extensively used as intercalators in DNA.[18−23] Its photophysical properties[20,24−27] are rather intriguing as are those of several similar systems containing pyridophenazine units.[28−33] The presence of an electron-withdrawing group, such as the phenazine moiety, and the weak electronic interaction between this unit and the phenanthroline chelating site have attracted a lot of attention. Furthermore, the existence of more MLCT excited states and their possible equilibrium has been recently described.[30,32]

Here we report the syntheses, the electrochemical and photophysical properties of two luminescent bimetallic complexes, containing ruthenium and osmium units, and of the bridging ligand linking the two metal complexes. The bridging ligand is 1,1′-dipyrido[3,2-*a*:2′,3′-*c*]phenazin-1,1′-yldipyrido[3,2-*a*:2′,3′-*c*]phenazine (bidppz),[34,35] which consists of two dppz moieties linked by a single C−C bond (Chart 1). The two metal units have ancillary 2,2′-bipyridine ligands, and the homometallic complexes are indicated hereinafter as [Ru-bidppz-Ru]$^{4+}$ and [Os-bidppz-Os]$^{4+}$ (Chart 1). The monometallic [Ru-dppz]$^{2+}$ complex (Chart 1) will also be discussed, as a reference compound. By time-resolved spectroscopic investigations performed in a wide time resolution range (from subpico- to microsecond) and in different solvents, insight into the excited states responsible for the spectroscopic behavior of the two complexes is obtained.

Experimental Section

Materials. All solvents and reagents used in the preparations were reagent grade, purchased from Fluka or Aldrich, and used as supplied. Silica gel preparative plates and aluminum oxide chromatographic columns were used for purification of the metal complexes. The preparative SiO_2 plates were made of silica gel purchased from Merck (60, particle size 0.040−0.063 mm) and prepared according to the procedure indicated by Merck. Aluminum oxide for chromatography was purchased from Fluka (Type 507 C neutral, Brockmann Grade I, particle size 0.05−0.15 mm, pH 7.0 ± 0.5). For electrochemistry and spectroscopy, butyronitrile (Acros) was dried over CaH_2 and freshly distilled under nitrogen prior to use. For spectroscopy, acetonitrile, dichloromethane, ethanol, and methanol (Fluka, spectroscopic grade) were used as received. The supporting electrolyte Bu_4-

* Corresponding author. Telephone: +31-(0)20-5256459. Fax: +31-(0)20-5256456. Email: ldc@science.uva.nl.
[†] Universiteit van Amsterdam.
[‡] University of Fribourg.

10.1021/jp026002i CCC: $22.00
Published on Web 09/17/2002

CHART 1: Schematic Formulas of the Investigated Compounds and Their Abbreviations[a]

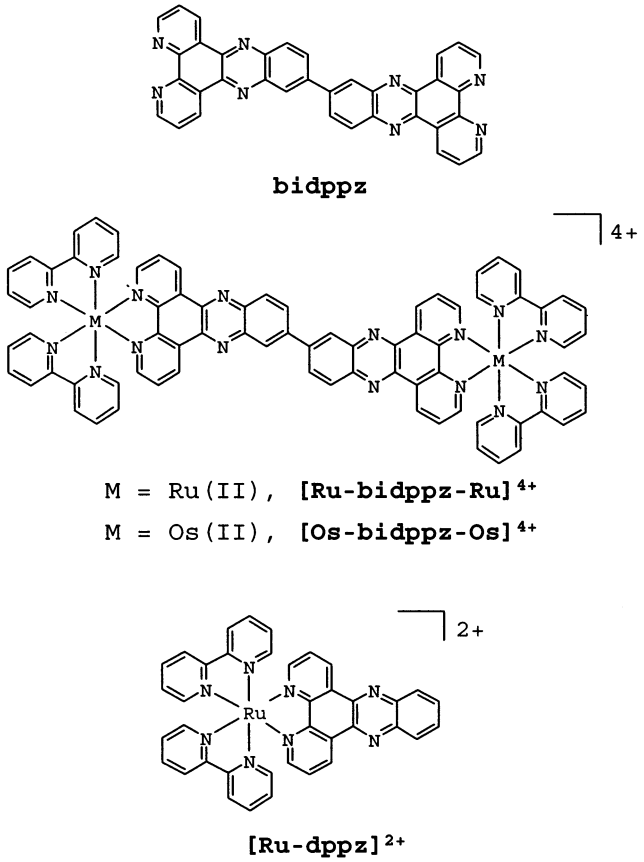

[a] The reference complex $[Ru\text{-}dppz]^{2+}$ is also shown.

NPF_6 (Aldrich) was recrystallized twice from ethanol and dried overnight under reduced pressure at 60 °C. Ferrocene (Aldrich) was used as supplied.

Syntheses. The compounds bidppz,[35] [Ru-bidppz-Ru]$(PF_6)_4$,[35] and $[Os(bpy)_2Cl_2]$[36] were prepared according to literature procedures.

$[\{Os(bpy)_2\}_2(\mu\text{-bidppz})](PF_6)_4$, [Os-bidppz-Os]$^{4+}$. $[Os(bpy)_2Cl_2]$ (0.115 g, 0.2 mmol), bidppz (0.056 g, 0.1 mmol), and 2 drops of hexafluorophosphoric acid (60 wt % solution in water) were suspended in ethylene glycol (6 mL) and heated in a microwave oven (8 times for 2 min). The solvent was removed under reduced pressure, and then water (20 mL) and NH_4PF_6 (1 g) were added to give a dark olive precipitate that was separated by suction filtration. The crude product was purified on a column of neutral aluminum oxide (10 × 2 cm) with acetone/water 98:2 as eluent. The olive-brown band (TLC: R_f = 0.17, support SiO_2, solvent $MeCN/H_2O/MeOH/KNO_3$ 4:1:1:0.1) was collected, the solvents were removed under reduced pressure, and the residual solid was further purified on SiO_2 plates ($MeCN/H_2O$/*tert*-butyl alcohol/KNO_3 4:1:1:0.1). Isolation (with acetone/NH_4PF_6 99:1 as eluent) of the dark olive-brown band gave the pure product (0.060 g, 28%). ^1H NMR (CD_3CN): bpy signals δ = 7.19 (dd, 2 H, H11), 7.39 (dd, 2 H, H11′), 7.66 (d, 2 H, H10); 7.78 (d, 2 H, H10′), 7.85 (dd, 2 H, H12), 7.94 (dd, 2 H, H12′), 8.52 (d, 2 H, H13), 8.55 (d, 2 H, H13′); bidppz signals δ = 7.83 (dd, 2 H, H2 and H8), 8.13 (d, 2 H, H1 and H9), 8.67 (d, 1 H, H6), 8.75 (d, 1 H, H5), 9.03 (s, 1 H, H4), 9.45 (d, 1 H, H7), 9.48 (d, 1 H, H3). See Chart 2 for proton numbering. MS/ESI, m/z = 929.13 $[M^+ - 2PF_6^-]$, 571.10 $[M^+ - 3PF_6^-]$, 392.09 $[M^+ - 4PF_6^-]$; HRMS for $C_{76}H_{50}N_{16}Os_2$: calcd 392.0895; found 392.0881.

CHART 2

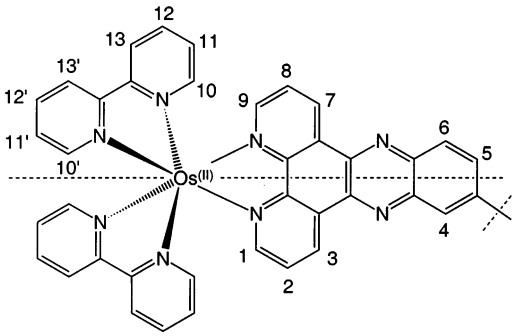

General Techniques. ^1H NMR spectra were recorded on a Varian Gemini 300 (300.075 MHz) spectrometer; chemical shifts are given in ppm, using the solvent itself as internal standard. Attribution of the ^1H signals was performed by the COSY technique. The numbering of the protons of the metal complexes is shown in Chart 2. ESI (electron spray ionization) mass spectra were measured with a Bruker FTMS 4.7 T Bio APEXII spectrometer.

Cyclic and differential pulse voltammetric scans were performed with a gastight single-compartment cell under an atmosphere of dry nitrogen or argon. The cell was equipped with a Pt disk working (apparent surface area of 0.42 mm^2), Pt wire auxiliary, and Ag wire pseudoreference electrodes. The working electrode was carefully polished with a 0.25 μm grain diamond paste between scans. The potential control was achieved with a PAR Model 283 potentiostat. All redox potentials are reported against the ferrocene−ferrocenium (Fc/Fc^+) redox couple used as an internal standard[37] ($E_{1/2}$ = 0.42 V vs SCE in acetonitrile). Tetrabutylammonium hexafluorophosphate (Bu_4NPF_6) was used as supporting electrolyte.

UV−vis spectroelectrochemical experiments were performed with an optically transparent thin-layer electrochemical (OTTLE) cell,[38] equipped with a Pt minigrid working electrode and quartz optical windows. The controlled-potential electrolyses were carried out with a PA4 potentiostat (EKOM, Czech Republic). All electrochemical samples were 5×10^{-4} M in the studied complex and contained 3×10^{-1} M Bu_4NPF_6.

UV−vis spectra were recorded on a Hewlett-Packard 8453 diode-array spectrophotometer. Emission and excitation spectra were recorded on a Spex 1681 spectrophotometer. All the emission spectra are corrected for the photomultiplier response.

Nanosecond time-resolved absorption spectra were obtained using a setup described previously.[39] The irradiation source was a continuously tunable (400−700 nm) Coherent Infinity XPO laser working at 10 Hz (2 ns fwhm). A 50% mirror was used to divide the probe light, sending one part through the excited sample and one part through a reference cuvette, which greatly improved the signal-to-noise ratio. Using the 50% mirror, the noise due to variable inhomogeneity of the probe light could be avoided. Excitation laser light was typically less than 5 mJ $pulse^{-1}$. Samples were prepared to have optical density, at the excitation wavelength, of ca. 0.3 in a 1 cm cuvette. For each sample, spectra were measured at not less than 25 different time delays.

Time-resolved emission studies were performed at a single wavelength using a continuously tunable (400−700 nm) Coherent Infinity XPO laser as excitation source. The emitted light was collected in an Oriel monochromator, detected by a P28 PMT (Hamamatsu), and recorded on a Tektronix TDS3052 (500 MHz) oscilloscope. A photodiode was used as external trigger source. Alternatively, a streak camera (Hamamatsu C5680-21),

TABLE 1: Electrochemical Data of the Investigated Complexes and Reference Compounds[a]

complex	bidppz$^{2-/1-}$	bpy$^{1-/0}$	bidppz$^{2-/1-}$	bidppz$^{1-/0}$	dppz$^{1-/0}$	Ru$^{II/III}$	Os$^{II/III}$
[Ru-bidppz-Ru]$^{4+}$	−2.26 (1)	−1.80 (2) −2.04 (2)	−1.42 (1)	−1.23 (1)		+0.91 (2)	
[Os-bidppz-Os]$^{4+}$	−2.23 (1)	−1.74 (2) −2.03 (2)	−1.41 (1)	−1.22 (1)			+0.47 (2)
[Ru-dppz]$^{2+}$		−1.80 (1) −2.06 (1)			−1.39 (1)	+0.94 (1)	
[Ru(bpy)$_3$]$^{2+}$		−1.72 (1) −1.93 (1)				+0.89 (1)	
[Os(bpy)$_3$]$^{2+}$		−1.59 (1) −1.77 (1)					+0.45 (1)

[a] Redox potentials ($E_{1/2}$) in volts vs Fc/Fc$^+$, in butyronitrile at 293 K. In parentheses, the number of transferred electrons.

equipped with an M 5677 sweep unit was used, with a continuously tunable (400−700 nm) Coherent Infinity XPO laser as excitation source.

(Sub)picosecond transient absorption spectra and single-wavelength kinetics were measured using a setup described in detail in a previous paper.[40] The laser system was based on a Spectra-Physics Hurrican titanium sapphire regenerative amplifier system. The full spectrum setup was based on an optical parametric amplifier (Spectra-Physics OPA 800) as a pump. A residual fundamental light, from the pump OPA, was used for white light generation, which was detected with a CCD spectrograph. The single wavelength kinetics measurements setup was based on two OPAs, one used for pumping and the other one for probing, and an amplified Si photodiode for detection. For both setups the OPA was used to generate excitation pulses at 350 nm. The laser output was typically 5 μJ pulse^{-1} (130 fs fwhm) with a repetition rate of 1 kHz. A circular cuvette (d = 1.8 cm, 1 mm, Hellma), with the sample solution, was placed in a homemade rotating ball bearing (1000 rpm), to avoid local heating by the laser beam. The solutions of the samples were prepared to have an optical density at the excitation wavelength of ca. 0.5 in a 1 mm cell. The absorbance spectra of the solutions were measured before and after the experiments. In all cases less than 10% photodecomposition was observed.

Luminescence quantum yields were measured in optically dilute solutions, using [Ru(bpy)$_3$]Cl$_2$ in H$_2$O (Φ_{em} = 0.028)[41] as reference emitter. Estimated experimental errors in the reported data are as follows: absorption and emission maxima ± 2 nm; emission lifetimes 8%; emission quantum yields ± 20%. Where required, deaerated solutions were prepared by freeze−pump−thaw technique on a vacuum line.

Results

Electrochemistry. The electrochemical data for compounds [Ru-bidppz-Ru]$^{4+}$ and [Os-bidppz-Os]$^{4+}$, and the reference compounds [Ru-dppz]$^{2+}$, [Ru(bpy)$_3$]$^{2+}$, and [Os(bpy)$_3$]$^{2+}$, are summarized in Table 1. The cyclic and differential pulse voltammograms (CV and DPV) for [Ru-bidppz-Ru]$^{4+}$ have been reported in a previous communication.[35] Complex [Os-bidppz-Os]$^{4+}$ undergoes multiple reduction at −1.22, −1.41, −1.74, −2.03, and −2.23 V. Based on the integrated DPV current intensities, the reversible reduction steps at −1.22, −1.41 and −2.23 V correspond to the transfer of one electron, and the cathodic waves at −1.74 and −2.03 V are two-electron-reduction processes. The electrochemical behavior of [Os-bidppz-Os]$^{4+}$ in the cathodic region is much like that of the analogous bimetallic ruthenium complex, [Ru-bidppz-Ru]$^{4+}$ (Table 1). In the anodic region, [Os-bidppz-Os]$^{4+}$ exhibits a reversible two-electron oxidation at $E_{1/2}$ = +0.47 V, which is less positive, by 440 mV, than the oxidation of [Ru-bidppz-Ru]$^{4+}$. Such a potential difference is commonly observed for other isostructural osmium and ruthenium complexes.[42,43]

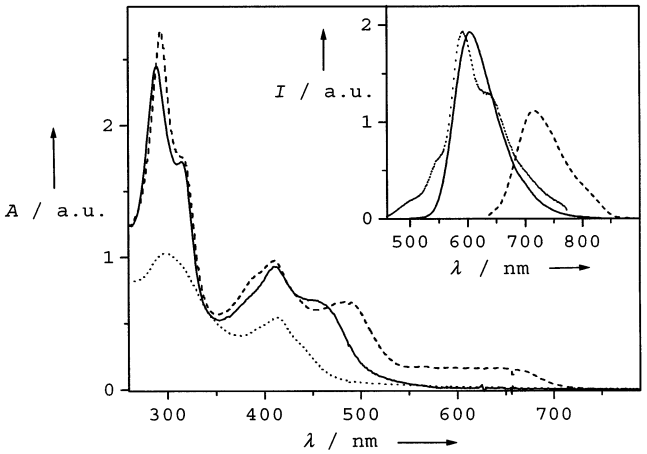

Figure 1. UV−vis spectra of [Ru-bidppz-Ru]$^{4+}$ (—), [Os-bidppz-Os]$^{4+}$ (---), and bidppz (•••) in CH_2Cl_2. Inset: Room-temperature emission spectra of [Ru-bidppz-Ru]$^{4+}$ (—) and [Os-bidppz-Os]$^{4+}$ (---) in CH_2Cl_2 (excitation wavelength 460 nm), and 77 K phosphorescence of bidppz (•••) in MeOH /EtOH matrix containing $ZnCl_2$ (excitation wavelength 350 nm).

TABLE 2: Absorption Data of the Investigated Compounds in CH_2Cl_2

complex	λ_{abs}/nm ($\epsilon \times 10^{-4}$/dm^3 mol^{-1} cm^{-1})
[Ru-bidppz-Ru]$^{4+}$	289 (13.7), 410 (5.5), 464 (sh, 3.2)
[Os-bidppz-Os]$^{4+}$	293 (15.9), 410 (5.8), 490 (3.4), 580 (1.1)
[Os-bidppz-Os]$^{3+}$	293 (13.6), 375 (4.7), 490 (4.0), 584 (2.8)
[Os-bidppz-Os]$^{2+}$	293 (12.5), 360 (5.0), 496 (3.7), 580 (2.0), 980 (3.8)
bidppz	297, 413

UV−vis Absorption. The UV−vis absorption spectra of the investigated compounds [Ru-bidppz-Ru]$^{4+}$ and [Os-bidppz-Os]$^{4+}$ and the ligand bidppz in dichloromethane are depicted in Figure 1. Changing the solvent to acetonitrile causes only minor changes. The UV−vis absorption data are summarized in Table 2. Due to the poor solubility in all common solvents, the absorption molar coefficients of the ligand bidppz could not be determined with precision.

The UV−vis absorption spectra were also recorded for one- and two-electron-reduced diosmium complexes, [Os-bidppz-Os]$^{n+}$ with n = 3 and 2, respectively, in butyronitrile within an optically transparent thin-layer electrochemical (OTTLE)[38] cell. The absorption data of the redox products are summarized in Table 2. Upon one-electron reduction, the shoulder observed for [Os-bidppz-Os]$^{4+}$ at ca. 320 nm and the band at 410 nm decrease in intensity, while the band at ca. 580 nm increases and a new band arises at 375 nm. Upon the second one-electron reduction, the band at ca. 580 nm decreases and a new intense low-lying absorption band[35] arises at 980 nm.

TABLE 3: Emission Data of the Investigated Complexes and Reference Compounds

	RT[a]					
	in CH_2Cl_2		in BuCN		77 K in BUCN	
complex	λ_{em}, nm	τ, ns	λ_{em}, nm	τ, ns	λ_{em}, nm	τ, μs
[Ru-bidppz-Ru]$^{4+}$	613	9700	675	360	591	4.0
[Os-bidppz-Os]$^{4+}$	750	16			730	0.68
bidppz[b]				27000[c]	421 (fl), 586 (ph)[d]	5.2
[Ru-dppz]$^{2+}$	600	590	624	500	581	5.0
[Ru(bpy)$_3$]$^{2+}$	600		610	1100[e]	579	5.1[c]
[Os(bpy)$_3$]$^{2+}$	717		733	60[f]	700	1.1

[a] Deaerated solutions. [b] Solutions containing $ZnCl_2$. [c] Data from time-resolved transient absorption measurements in CH_3CN. [d] Data in EtOH/MeOH (4:1). [e] Reference 31. [f] Reference 49.

Emission. Photophysical data of the investigated compounds [Ru-bidppz-Ru]$^{4+}$ and [Os-bidppz-Os]$^{4+}$ and the ligand bidppz are summarized in Table 3. The reference compounds [Ru-dppz]$^{2+}$, [Ru(bpy)$_3$]$^{2+}$, and [Os(bpy)$_3$]$^{2+}$ are also included for comparison.

The emission spectra of [Ru-bidppz-Ru]$^{4+}$ and [Os-bidppz-Os]$^{4+}$ in dichloromethane at room temperature were recorded upon excitation at 460 nm (inset Figure 1). At room temperature, the compound [Ru-bidppz-Ru]$^{4+}$ exhibits a maximum at 613 nm, slightly red-shifted with respect to the reference complexes [Ru(bpy)$_3$]$^{2+}$ and [Ru-dppz]$^{2+}$. Surprisingly, the excited-state lifetime of [Ru-bidppz-Ru]$^{4+}$ in deaerated dichloromethane solution is very long, 9.7 μs. This value significantly exceeds the lifetime of 590 ns determined for the model compound [Ru-dppz]$^{2+}$ under the same experimental conditions. Variation of the solvent strongly influences the emission properties of [Ru-bidppz-Ru]$^{4+}$. In deaerated butyronitrile solution the lifetime drops to 360 ns, a value similar to that for the reference compound [Ru-dppz]$^{2+}$ (500 ns), and the emission maximum is red-shifted to 675 nm. The emission of [Ru-bidppz-Ru]$^{4+}$ in dichloromethane is very sensitive to the presence of dioxygen, and the excited-state lifetime is reduced to 800 ns in air-equilibrated solution, while in butyronitrile, where the lifetime is already much shorter, the effect is smaller (210 ns, in air-equilibrated solution). The analogous bimetallic osmium complex [Os-bidppz-Os]$^{4+}$ shows, in dichloromethane, an emission maximum at 750 nm, red-shifted with respect to [Os(bpy)$_3$]$^{2+}$ complex, which emits at 717 nm. The lifetime of [Os-bidppz-Os]$^{4+}$ is 16 ns, in deaerated solution. In butyronitrile, the emission maximum of [Os-bidppz-Os]$^{4+}$ shifts toward the near-infrared region and becomes so weak to prevent an accurate lifetime determination. The emission of [Ru-bidppz-Ru]$^{4+}$ and [Os-bidppz-Os]$^{4+}$ does not show any dependence on the excitation wavelength. Emission quantum yields have been determined for [Ru-bidppz-Ru]$^{4+}$ in deaerated dichloromethane and butyronitrile solutions: 0.005 and 0.025, respectively.

The emission spectra of [Ru-bidppz-Ru]$^{4+}$ and [Os-bidppz-Os]$^{4+}$ were also recorded in butyronitrile at 77 K, by excitation at 460 nm. The ruthenium complex [Ru-bidppz-Ru]$^{4+}$ exhibits structured emission with a maximum centered at 591 nm, slightly red-shifted with respect to the reference complexes [Ru-dppz]$^{2+}$ and [Ru(bpy)$_3$]$^{2+}$, emitting at ca. 580 nm (Table 3). The emission lifetime of [Ru-bidppz-Ru]$^{4+}$ is 4 μs, a value similar to the 5 μs lifetime determined for the reference complexes, but also similar to the free ligand (Table 3). At 77 K in butyronitrile matrix the osmium complex [Os-bidppz-Os]$^{4+}$ emits at 730 nm with lifetime of 680 ns (Table 3). The uncoordinated bridging ligand bidppz shows broad fluorescence and phosphorescence bands at 473 and 590 nm, respectively, at 77 K in MeOH/EtOH 1:4 (v/v) matrix upon excitation at 350 nm. In the presence of a large excess of $ZnCl_2$, the fluorescence and phosphorescence of bidppz become structured and shift to 421 and 586 nm, respectively (Table 3, inset Figure 1).

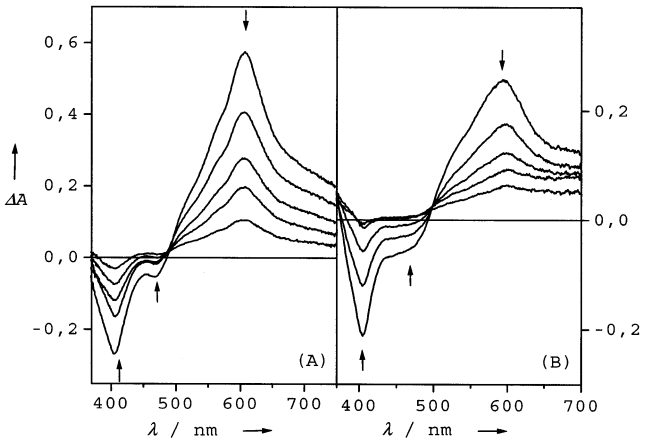

Figure 2. (A) Difference transient absorption spectra of [Ru-bidppz-Ru]$^{4+}$ in deoxygenated CH_2Cl_2 solution, measured at time delays of 0, 3, 6, 9, and 15 μs, respectively (λ_{exc} = 460 nm, 2 ns fwhm). (B) Difference transient absorption spectra of [Ru-bidppz-Ru]$^{4+}$ in deoxygenated butyronitrile solution, measured at time delays of 0, 200, 400, 600, and 800 ns, respectively (λ_{exc} = 460 nm, 2 ns fwhm).

Excitation spectra of [Ru-bidppz-Ru]$^{4+}$ and [Os-bidppz-Os]$^{4+}$ were recorded at 610 and 700 nm, respectively, in dichloromethane. They closely resemble the profile of the absorption spectra of these compounds.

Micro- and Nanosecond Time-Resolved Transient Absorption Spectra. Transient absorption (TA) spectra of [Ru-bidppz-Ru]$^{4+}$ and [Os-bidppz-Os]$^{4+}$ in the micro- and nanosecond time domains were recorded upon excitation at 460 nm (2 ns fwhm). The TA spectra of [Ru-bidppz-Ru]$^{4+}$ in deaerated dichloromethane and butyronitrile are depicted in parts A and B, respectively, of Figure 2. The TA spectra of [Os-bidppz-Os]$^{4+}$, recorded in deoxygenated dichloromethane, are shown in Figure 3. For the bridging ligand bidppz, TA spectra were measured in the microsecond time domain in deoxygenated acetonitrile, by excitation at 435 nm (2 ns fwhm) (Figure 4).

In deoxygenated dichloromethane solution, [Ru-bidppz-Ru]$^{4+}$ shows the bleach of the ground state between 380 and 480 nm, while an intense transient absorption band arises at ca. 600 nm. The transient absorption band and the bleach of the ground-state decay with first-order kinetics and lifetime of about 9 μs, similar to the corresponding emission decay (see above). The intensity of the transient band is unusually high, compared to transient absorption bands observed for other ruthenium monometallic[27,44] and bimetallic complexes.[31] The ns-TA spectra of [Ru-bidppz-Ru]$^{4+}$ in butyronitrile show ground-state bleach in the region 380−480 nm and a transient absorption band at 594 nm (Figure 2B) that decays with τ of ca. 350 ns, following a first-order kinetics. This decay time is similar to the emission

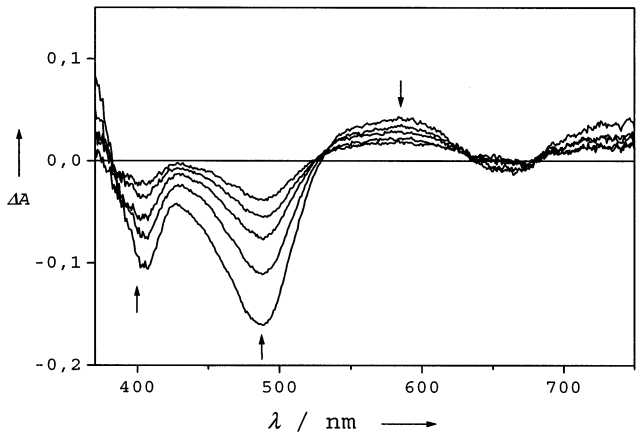

Figure 3. Difference transient absorption spectra of [Os-bidppz-Os]$^{4+}$ in deoxygenated CH_2Cl_2 solution, measured at time delays of 0, 5, 10, 15, and 20 ns, respectively (λ_{exc} = 460 nm, 2 ns fwhm).

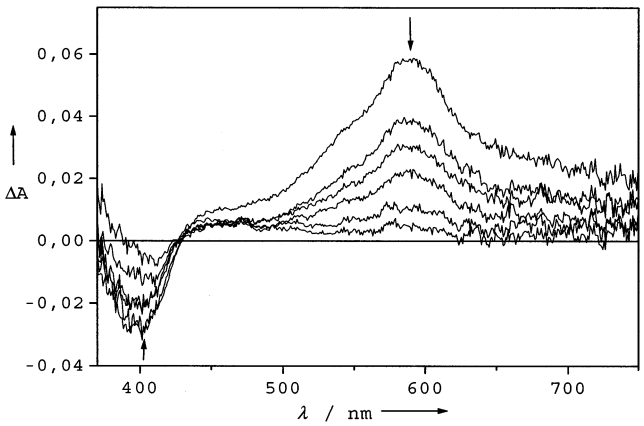

Figure 4. Difference transient absorption spectra of bidppz in deoxygenated CH_2Cl_2 solution, measured at time delays of 0, 9, 18, 27, 36, and 54 μs, respectively (λ_{exc} = 460 nm, 2 ns fwhm).

lifetime in the same solvent (see above). The profile of the band at 594 nm differs from that of the band at 600 nm observed for [Ru-bidppz-Ru]$^{4+}$ in dichloromethane. Furthermore, the intensity of the 594 nm band is rather weak, as it can be easily seen by the ratio between this absorption and the bleach at 404 nm (1:1 compared to 3:1 in dichloromethane). The different profiles and decays observed for the TA spectra in butyronitrile and dichloromethane suggest that the lowest excited state is not the same in these two solvents.

The ns-TA spectra of [Os-bidppz-Os]$^{4+}$ in dichloromethane strongly differ from the analogous ruthenium complex in the same solvent (Figure 3). The bleach of the ground state dominates the region between 400 and 480 nm, while a weak transient absorption is observed at 580 nm. The recovery of the ground state, monitored at 480 nm, follows a first-order kinetics with lifetime of 13 ns, similar to the emission decay (see above).

The TA spectra of ligand bidppz were measured in deoxygenated acetonitrile in the presence of a large excess of $ZnCl_2$ (Figure 4). Besides the increase of solubility of the ligand, the coordination of bidppz to Zn^{2+} allows a better comparison of the properties of the ligand with the Ru(II) and Os(II) metal complexes, when it is coordinated with a divalent ion. Importantly, transient absorption of the ligand arises at 590 nm, with a profile very similar to the band observed for [Ru-bidppz-Ru]$^{4+}$ in dichloromethane at ca. 600 nm. The transient absorption band at 590 nm decays with a lifetime of 27 μs, following a first-order kinetics.

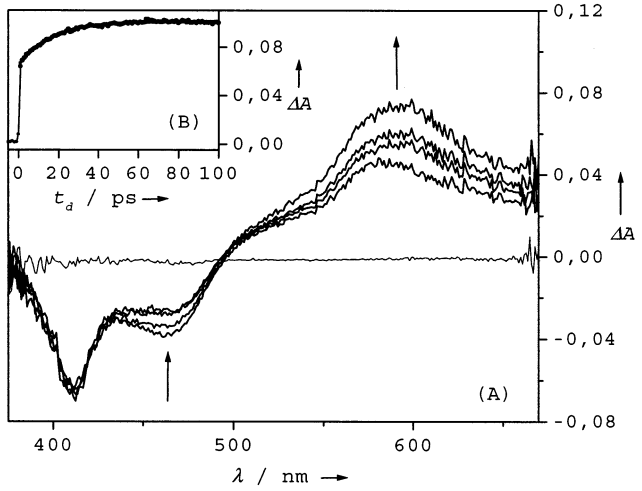

Figure 5. (A) Difference transient absorption spectra of [Ru-bidppz-Ru]$^{4+}$ in CH_2Cl_2 solution, measured at time delays of 0, 6, 12, and 36 ps, respectively (λ_{exc} = 350 nm, 130 fs fwhm). (B) Kinetic profile of the difference absorbance, measured at 610 nm with 1 ps increment delay (λ_{exc} = 350 nm, 130 fs fwhm).

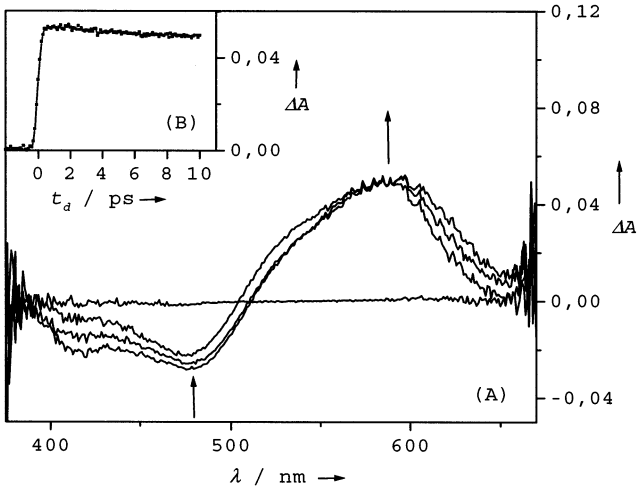

Figure 6. (A) Difference transient absorption spectra of [Ru-bidppz-Ru]$^{4+}$ in butyronitrile solution, measured at time delays of 0 (baseline), 5, 20, and 30 ps, respectively (λ_{exc} = 350 nm, 130 fs fwhm). (B) Kinetic profile of the difference absorbance, measured at 610 nm with 0.1 ps increment delay (λ_{exc} = 350 nm, 130 fs fwhm).

(Sub)picosecond Transient Absorption Spectra. Picosecond transient absorption (ps-TA) spectra were recorded for bimetallic complex [Ru-bidppz-Ru]$^{4+}$ in dichloromethane and in butyronitrile, and for [Os-bidppz-Os]$^{4+}$ in dichloromethane. Spectral changes after excitation at 350 nm were monitored between 380 and 680 nm. Kinetic profiles were probed at 610 nm (transient absorption) for compound [Ru-bidppz-Ru]$^{4+}$ and at 470 nm (bleaching) for compound [Os-bidppz-Os]$^{4+}$. The ps-TA spectra and kinetics of [Ru-bidppz-Ru]$^{4+}$ in dichloromethane and butyronitrile are depicted in Figures 5 and 6, respectively. Figure 7 shows the ps-TA spectra and kinetics of [Os-bidppz-Os]$^{4+}$ in dichloromethane.

The ps-TA spectrum of [Ru-bidppz-Ru]$^{4+}$ in dichloromethane measured 1 ps after the laser pulse (Figure 5A) shows bleach of the ground state in the region between 400 and 500 nm and transient absorption with the maximum at 580 nm. The kinetic profile recorded at 610 nm shows that the transient absorption band is partially formed by direct excitation within the instrumental rise time, and subsequently, its intensity increases in time (τ = 16 ps) due to indirect formation from another

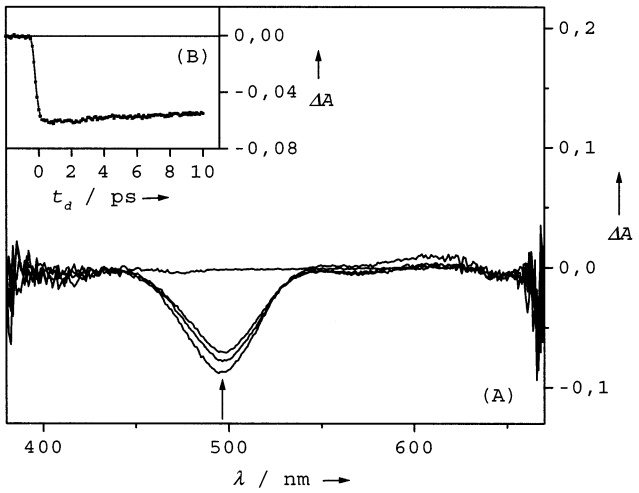

Figure 7. (A) Difference transient absorption spectra of [Os-bidppz-Os]$^{4+}$ in CH_2Cl_2 solution, measured at time delays of 0 (baseline), 1, 5, and 10 ps, respectively (λ_{exc} = 350 nm, 130 fs fwhm). (B) Kinetic profile of the difference absorbance, measured at 470 nm with 0.1 ps increment delay (λ_{exc} = 350 nm, 130 fs fwhm).

excited state (Figure 5B). The ratio between its direct and delayed formation is ca. 7:3 (Figure 5A). The bleach at 460 nm decreases with time, suggesting that the excited state absorbing at 580 nm develops from the excited state populated by the absorption of the ground state at 460 nm. The last spectrum recorded at 36 ps has the same profile as the ns-TA spectrum (see above).

In butyronitrile, the ps-TA spectrum of [Ru-bidppz-Ru]$^{4+}$ measured 5 ps after the laser pulse (Figure 6A) shows a bleach in the region between 400 and 500 nm and transient absorption band at 590 nm. The shape of this band is different from that observed in dichloromethane, with a profile significantly falling off at 650 nm. The kinetic plot recorded at 610 nm (Figure 6B) shows that the transient band is formed within the instrumental rise time and decays in the nanosecond time scale. The different kinetics and profiles observed for the transient band of [Ru-bidppz-Ru]$^{4+}$, in dichloromethane and butyronitrile, suggest that the corresponding excited states in the two solvents are different, in agreement with the observations made in the nanosecond time domain.

The ps-TA spectra of complex [Os-bidppz-Os]$^{4+}$ in dichloromethane are dominated by the bleach at 490 nm (Figure 7A). In the visible region no clear transient absorption can be observed. Kinetics plotted at 470 nm shows the formation of the bleach within the instrumental rise time and a slow recovery of the ground state on the nanosecond time scale (Figure 7B).

Discussion

Redox Properties. Cyclic and differential pulse voltammograms of [Ru-bidppz-Ru]$^{4+}$ [35] and [Os-bidppz-Os]$^{4+}$ are consistent with metal(II)-based oxidations and several ligand-based reductions.

In the cathodic region, the first two steps for [Ru-bidppz-Ru]$^{4+}$ and [Os-bidppz-Os]$^{4+}$ consume one electron each and occur at potentials close to the reduction of the dppz ligand in [Ru-dppz]$^{2+}$, far less negative than the reduction of the bipyridine ligands, e.g., in [Ru(bpy)$_3$]$^{2+}$ and [Os(bpy)$_3$]$^{2+}$ (Table 1). As was already well established, ligands such as dppz[45,46] and tpphz[33] (tpphz = tetrapyrido[3,2-*a*:2′,3′-*c*:3″,2″-*h*:2‴3‴-*j*]phenazine) have the lowest unoccupied molecular orbital (LUMO) mainly localized on their phenazine part, with negligible electron density on the two coordinating nitrogen atoms of their phenanthroline unit. By analogy, we can expect a similar situation for bidppz. This is consistent with the first two reduction steps localized on the phenazine moieties of the bridging ligand in [Ru-bidppz-Ru]$^{4+}$ and [Os-bidppz-Os]$^{4+}$. Furthermore, a poor electronic communication exists between the coordinated metal ions and the phenazine units, explaining the negligible effect of the nature of the metal ion on the first two reduction potentials in the two complexes. In contrast, the separation of the two cathodic waves of the bridging ligand points to a strong electronic communication between the two dppz moieties. The third and fourth steps of [Ru-bidppz-Ru]$^{4+}$ and [Os-bidppz-Os]$^{4+}$ occur as two bielectronic cathodic waves, with potentials similar to the first two reductions of the bpy ligands in [Ru(bpy)$_3$]$^{2+}$ and [Os(bpy)$_3$]$^{2+}$ (Table 1). Therefore, they are assigned to two pairwise one-electron reductions of the bipyridine ligands at the remote metal centers. The fifth step is assigned to one-electron reduction of the doubly reduced bridging ligand bidppz^{2-}.

In the anodic region, the two complexes [Ru-bidppz-Ru]$^{4+}$ and [Os-bidppz-Os]$^{4+}$ are oxidized at the metal centers in an unresolved doubly one-electron process. Such behavior again reveals a weak electronic communication between the two metals. The less positive oxidation potential of [Os-bidppz-Os]$^{4+}$ compared to [Ru-bidppz-Ru]$^{4+}$ is consistent with the higher energy of the 5d-osmium orbitals.[47,48]

Absorption and Emission Properties. The absorption spectrum of [Ru-bidppz-Ru]$^{4+}$ has already been discussed in some detail in a previous communication.[35] In the UV region, the absorption spectra of the two bimetallic complexes [Ru-bidppz-Ru]$^{4+}$ and [Os-bidppz-Os]$^{4+}$ show bands assigned to singlet intraligand (^{1}IL) absorption due to $\pi-\pi^*$ transitions of the ancillary bipyridines and of the bidppz ligand (Figure 1). The band at 410 nm, also present in the absorption spectrum of bidppz (Figure 1), is referred to a ^{1}IL transition within the bridging ligand, namely to the $\pi-\pi^*$ transition localized on the phenazine moiety. In the region of 440−540 nm, the electronic absorption spectra of the bimetallic metal complexes [Ru-bidppz-Ru]$^{4+}$ and [Os-bidppz-Os]$^{4+}$ show absorptions assigned to singlet metal-to-ligand charge-transfer (^{1}MLCT) transitions from the d_π orbitals of the metal to the π^* orbitals of the ancillary bipyridines and the phenanthroline part of the bridging ligand bidppz. Absorption due to ^{1}MLCT transitions from the d_π orbitals of the metal to the π^* orbital of the bidppz phenazine part is expected to be at the lowest energy, on the basis of the electrochemical data. However, due to the poor overlap of the d_π orbitals of the metal and the π^* orbital of the phenazine, the oscillator strength for this transition is too small to allow observation of the corresponding absorption band. The MLCT absorption bands of [Os-bidppz-Os]$^{4+}$ are red-shifted compared to the ruthenium complex. [Os-bidppz-Os]$^{4+}$ also shows a weak absorption tailing more to the red (540−680 nm), assigned to spin-forbidden electronic transitions (^{3}MLCT states) that become partially allowed due to the strong spin−orbit coupling in the osmium complexes.[49]

The emission maxima of [Ru-bidppz-Ru]$^{4+}$ and [Os-bidppz-Os]$^{4+}$ depend on the solvent polarity (Table 3). Solvatochromism is expected for metal complexes with the MLCT lowest excited state. However, for [Ru-bidppz-Ru]$^{4+}$ the change in solvent polarity has a dramatic change in emission properties. The luminescence of the bimetallic compound [Ru-bidppz-Ru]$^{4+}$ in butyronitrile is red-shifted compared to the reference complexes [Ru-dppz]$^{2+}$ and [Ru(bpy)$_3$]$^{2+}$, proving that its emitting excited state has more CT character, with the electron localized on a π^* orbital of the phenazine, lower than the lowest π^* orbital of the bpy and dppz. This result confirms what has already been

SCHEME 1: Simplified Energy Level Diagram of [Ru-bidppz-Ru]$^{4+}$ in CH_2Cl_2[a]

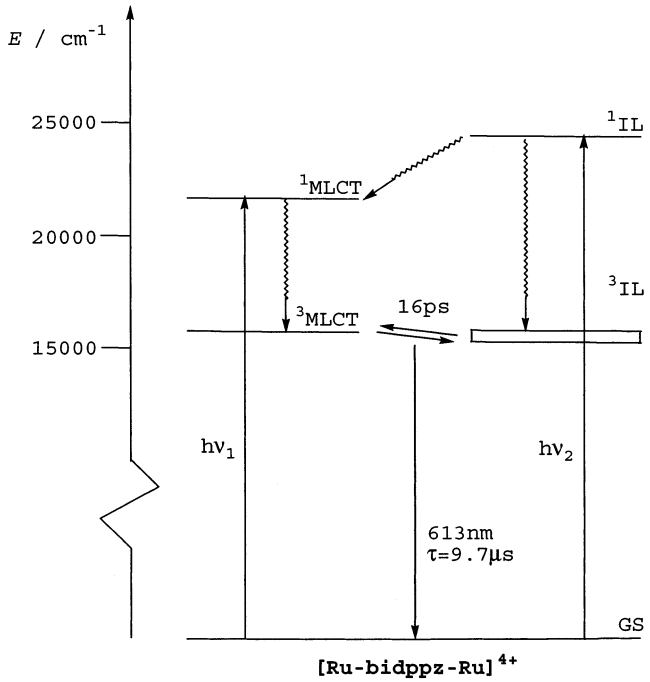

[a] Wavy arrows represent intersystem crossing and internal conversion decays; continuous arrows represent absorption and radiative decays.

deduced from the electrochemical data: the two phenazine moieties of bidppz are electronically coupled and the LUMO of the extended bidppz is low in energy. The lifetime of the emitting excited state of [Ru-bidppz-Ru]$^{4+}$ is of the same order of magnitude as the reference complex [Ru-dppz]$^{2+}$, consistent with their identical nature (^{3}MLCT), and in particular the shorter lifetime of the former is due to the lower energy emission, in agreement with the energy gap law. Changing solvent to the less polar dichloromethane, the emission maximum is blue-shifted to 613 nm, as expected for the polar character of the MLCT state (larger dipole moment in the excited state). However, the excited-state lifetime measured in deoxygenated solution is unusually long, 9.7 μs, for a pure MLCT state. The long lifetime cannot simply be attributed to the same emitting excited state observed in butyronitrile. The sensitivity toward dioxygen and the comparison with the phosphorescence of the free ligand suggest that a triplet ligand-centered state must be populated and is responsible for the long emission lifetime of the complex. In fact, the triplet state of the bidppz lies at about 17 065 cm^{-1}, very close in energy to the ^{3}MLCT excited state (16 920 cm^{-1}). In principle, the ^{3}IL state should still be at slightly higher energy, but due to the uncertainty in the position of the triplet state of the bidppz ligand (different metal ions and broad emission) and due to the low emission quantum yield and long lifetime of the emitting excited state in [Ru-bidppz-Ru]$^{4+}$, we believe that the lowest excited state of the dinuclear complex is indeed the ^{3}IL (see Scheme 1). The observed emission therefore results from an equilibrium between the ^{3}MLCT and the ^{3}IL states.

The shift of the emission observed for both [Ru-bidppz-Ru]$^{4+}$ and [Os-bidppz-Os]$^{4+}$ in a rigid butyronitrile matrix at 77 K compared to room temperature (Table 3) is consistent with the charge-transfer nature of the emitting excited state and the lack of solvent stabilization at low temperature. The bimetallic complex [Ru-bidppz-Ru]$^{4+}$ exhibits emission with spectral shape, energy, and lifetime similar to those of the monometallic complexes [Ru-dppz]$^{2+}$ and [Ru(bpy)$_3$]$^{2+}$. However, due to the similarity to the phosphorescence band and excited-state lifetime of the free bidppz (see Table 3 and Figure 1, inset), we cannot rule out a possible contribution from the ^{3}IL state. The emission of the bimetallic osmium complex [Os-bidppz-Os]$^{4+}$, in dichloromethane solution at room temperature, is attributed to a ^{3}MLCT state, where the electron is localized on the phenazine moiety of the bridging ligand, in agreement with the lower energy of the emitting excited state (750 nm) compared to [Os(bpy)$_3$]$^{2+}$ (emitting at 720 nm); see Table 3.

Time-Resolved Transient Absorption Spectroscopy. To investigate the electronic properties of the bimetallic compounds in more detail, transient absorption (TA) spectra in a large range of time domain were recorded. In the nanosecond time domain [Ru-bidppz-Ru]$^{4+}$, in deoxygenated butyronitrile solution, shows a transient band at 594 nm. A similar band is also observed in the steady-state absorption spectrum of the one-electron-reduced species [Ru-bidppz-Ru]$^{3+}$, at 590 nm.[35] The transient band can therefore be assigned to the absorption of the lowest ^{3}MLCT excited state where the electron is mainly localized on a phenazine moiety of the bridging ligand. Furthermore, the lifetime of ca. 350 ns of the transient band is typical for ^{3}MLCT excited states. In deaerated dichloromethane, the transient absorption band observed for [Ru-bidppz-Ru]$^{4+}$ at ca. 600 nm has a different shape and larger oscillator strength than in butyronitrile and, more importantly, a much longer (more than 20 times) decay time. Thus, the transient absorption band in dichloromethane cannot be assigned to the absorption of a pure ^{3}MLCT excited state. Interestingly, the TA spectra of the bridging ligand bidppz, in deoxygenated acetonitrile solution, show a transient absorption band at 590 nm with the shape and order of magnitude of the decay time similar to that of the bimetallic ruthenium complex [Ru-bidppz-Ru]$^{4+}$. The long-lived band observed for the ruthenium complex is therefore assigned to the absorption of the ^{3}IL(bidppz) state in thermal equilibrium with the higher lying ^{3}MLCT excited state (see Scheme 1), consistent with the emission data.

To have a mechanistic and kinetic understanding of the processes, [Ru-bidppz-Ru]$^{4+}$ was investigated by (sub)picosecond TA spectroscopy. In the ps-TA experiment the long-lived band observed in dichloromethane at about 580 nm is in part directly formed upon excitation and in part rises within 16 ps, to give ultimately a spectrum closely resembling that recorded on the microsecond time scale (Figure 5). The increase in intensity of this transient band is due to a delayed population of the ^{3}IL state from the energetically close ^{3}MLCT level, which is populated (after intersystem crossing ^{1}MLCT $\rightarrow$ ^{3}MLCT) upon excitation (see Scheme 1). This is in agreement with the decrease of the bleach at 450 nm, which indicates the population of, first, the ^{1}MLCT state and, subsequently, of the ^{3}IL state. The possibility of mixing the ^{3}IL and ^{3}MLCT states, in dichloromethane, is due to the small energy difference between the two states, estimated to 145 cm^{-1}. In our investigation no evidence for equilibrium between different MLCT states has been gained.[32] In butyronitrile the ps-TA spectra show direct formation of a transient absorption band at 594 nm that remains nearly unchanged during 100 ps after the laser pulse, in agreement with the direct population of the lowest ^{3}MLCT state involving the bridging ligand, which decays to the ground state in the nanosecond time domain. In butyronitrile solution the ^{3}MLCT state lies too low in energy (14 800 cm^{-1}) to allow any population of the higher lying ^{3}IL state (ΔE > 2000 cm^{-1}) (Scheme 2).

SCHEME 2: Simplified Energy Level Diagram of [Ru-bidppz-Ru]$^{4+}$ in Butyronitrile[a]

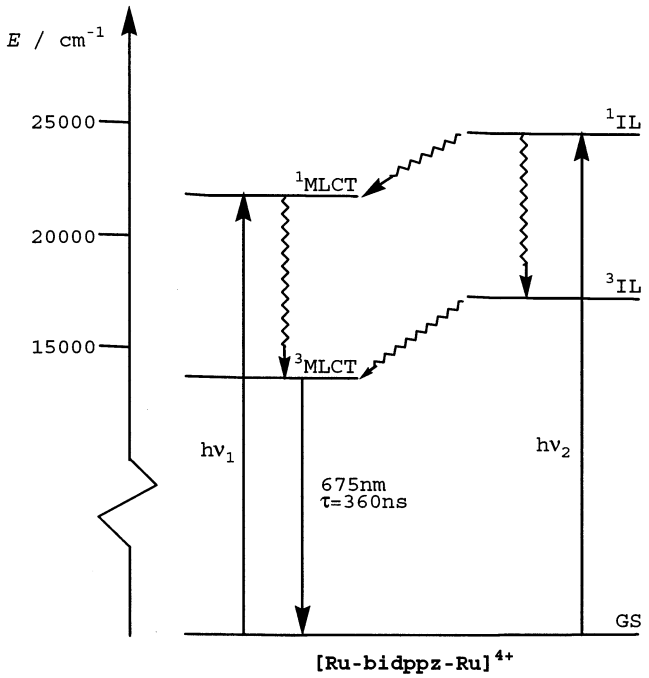

[a] Wavy arrows represent intersystem crossing and internal conversion decays; continuous arrows represent absorption and radiative decays.

The ns-TA spectra of the osmium bimetallic complex [Os-bidppz-Os]$^{4+}$ in dichloromethane are characterized by the bleach at the 400−480 nm region and a weak transient absorption band at ca. 580 nm. This band is assigned to the absorption of the lowest lying ^{3}MLCT state, with the excited electron mainly localized on the central phenazine part of the bridging ligand. The band at ca. 580 nm has a lower intensity than expected for the absorption band of the one-electron-reduced phenazine moiety. This is probably due to its overlap with the bleach of the ^{3}MLCT bands. The ps-TA spectra of complex [Os-bidppz-Os]$^{4+}$ are consistent with the TA spectra in the nanosecond time domain. The bleach of the ground state is formed within the laser pulse and remains nearly unchanged within 100 ps. This is in agreement with rapid population of the ^{3}MLCT excited state and its simple decay to the ground state on the nanosecond time scale.

Conclusions

We have synthesized and investigated the bimetallic ruthenium and osmium complexes, [Ru-bidppz-Ru]$^{4+}$ and [Os-bidppz-Os]$^{4+}$, and the bridging ligand bidppz (bidppz = 1,1′-dipyrido[3,2-*a*:2′,3′-*c*]phenazin-1,1′-yldipyrido[3,2-*a*:2′,3′-*c*]phenazine). From time-resolved spectroscopy, from subpico- to microsecond time domains, we have shown that different excited states are responsible for the spectroscopic behavior of the complexes in different solvents. In particular, for [Ru-bidppz-Ru]$^{4+}$ in butyronitrile the photoexcitation of the complex yields the population of a ^{3}MLCT state lying at lower energy than the ^{3}IL state of the bridging ligand bidppz, and it decays with a lifetime of 350 ns (Scheme 2). In deaerated dichloromethane solution, upon excitation, population of the ^{3}MLCT state is observed that establishes in 16 ps a thermal equilibrium with a higher lying ^{3}IL state. The interconversion rate between the ^{3}MLCT and ^{3}IL states is therefore $k = 6.2 \times 10^{10}$ s^{-1}. The emission occurs from the ^{3}MLCT state, equilibrated with the ^{3}IL state, and with a lifetime of 9.7 μs (Scheme 1). For the bimetallic osmium compound [Os-bidppz-Os]$^{4+}$, the ^{3}MLCT state lies too low in energy to be in equilibrium with the ^{3}IL state, in analogy to what observed for the ruthenium complex in butyronitrile.

The detailed mechanistic study has shown the richness and complexity of intramolecular photoinduced processes in rather simple homonuclear ruthenium and osmium compounds. The investigation, from subpico- to microsecond time scale, of the spectroscopy of the metal complexes allowed a deeper understanding of the intimate properties of the systems. The gained knowledge can now be used for a better design and comprehension of more complex and extended structures.

Acknowledgment. The authors thank the European Commission for the Marie Curie Individual Fellowship (Contract No. ERBFMBICT983052).

References and Notes

(1) *Coord. Chem. Rev.* Special issue on "Luminescent Sensors"; Fabbrizzi, L., Guest Ed.; **2000**, *205*.

(2) Malins, C.; Glever, H. G.; Keyes, T. E.; Vos, J. G.; Dressick, W. J.; MacCraith, B. D. *Sens. Actuators, B* **2000**, *67*, 89−95.

(3) De Silva, A. P.; Gunaratne, H. Q. N.; Gunnlaugsson, T.; Huxley, J. M.; McCoy, C. P.; Rademacher, J. T.; Rice, T. E. *Chem. Rev.* **1997**, *97*, 1515−1566.

(4) Moucheron, C.; Kirsch-De Mesmaeker, A.; Kelly, J. M. *J. Photochem. Photobiol., B* **1997**, *40*, 91−106.

(5) Murphy, C. J.; Barton, J. K. *Methods Enzymol.* **1993**, *226*, 576−594.

(6) *Chem. Rev.* Special issue on "Medicinal Inorganic Chemistry"; Orvig, C., Abrams, M. J., Guest Eds.; **1999**, *99*, 2201.

(7) Lee, W.-Y. *Mikrochim. Acta* **1997**, *127*, 19−39.

(8) Albano, G.; Belser, P.; De Cola, L.; Gandolfi, M. T. *Chem. Commun.* **1999**, *13*, 1171−1172.

(9) Treadway, J. A.; Loeb, B.; Lopez, R.; Anderson, P. A.; Keene, F. R.; Meyer, T. J. *Inorg. Chem.* **1996**, *35*, 2242−2246.

(10) Wilson, G. J.; Launikonis, A.; Sasse, W. H. F.; Mau, A. W.-H. *J. Phys. Chem. A* **1997**, *101*, 4860−4866.

(11) Simon, J. A.; Curry, S. L.; Schmehl, R. H.; Schatz, R. H.; Piotrowiak, P.; Jin, X.; Thummel, R. P. *J. Am. Chem. Soc.* **1997**, *119*, 11012−11022.

(12) Tyson, D. S.; Castellano, F. N. *J. Phys. Chem. A* **1999**, *103*, 10955.

(13) Sohna, J. E. S.; Carrier, V.; Fages, F.; Amouyal, E. *Inorg. Chem.* **2001**, *40*, 6061−6063.

(14) Fages, F.; Leroy, S.; Soujanya, T.; Sohna, J. E. S. *Pure Appl. Chem.* **2001**, *73*, 411−414.

(15) Del Guerzo, A.; Leroy, S.; Fages, F.; Schmehl, R. H. *Inorg. Chem.* **2002**, *41*, 359−366.

(16) McClenaghan, N. D.; Barigelletti, F.; Maubert, B.; Campagna, S. *Chem. Commun.* **2002**, *6*, 602−603.

(17) Tyson, D. S.; Luman, C. R.; Zhou, X.; Castellano, F. N. *Inorg. Chem.* **2001**, *40*, 4063−4071.

(18) Friedman, A. E.; Chambron, J.-C.; Sauvage, J.-P.; Turro, N. J.; Barton, J. K. *J. Am. Chem. Soc.* **1990**, *112*, 4960−4962.

(19) Kane-Maguire, N. A. P.; Wheeler, J. F. *Coord. Chem. Rev.* **2001**, *211*, 145−162.

(20) Coats, C. G.; Callaghan, P.; McGarvey, J. J.; Kelly, J. M.; Jacquet, L.; Mesmaeker, A. K.-D. *J. Mol. Struct.* **2001**, *598*, 15−25.

(21) Holmlin, R. E.; Yao, J. A.; Barton, J. K. *Inorg. Chem.* **1999**, *38*, 174−189.

(22) Holmlin, R. E.; Stemp, E. D. A.; Barton, J. K. *J. Am. Chem. Soc.* **1996**, *118*, 5236−5244.

(23) Stoeffler, H. D.; Thornton, N. B.; Temkin, S. L.; Schanze, K. S. *J. Am. Chem. Soc.* **1995**, *117*, 7119−7128.

(24) Chen, W.; Turro, C.; Friedman, L. A.; Barton, J. K.; Turro, N. J. *J. Phys. Chem. B* **1997**, *101*, 6995−7000.

(25) Olson, E. J. C.; Hu, D.; Hörmann, A.; Jonkman, A. M.; Arkin, M. R.; Stemp, E. D. A.; Barton, J. K.; Barbara, P. F. *J. Am. Chem. Soc.* **1997**, *119*, 11458−11467.

(26) Schoonover, J. R.; Bates, W. D.; Meyer, T. J. *Inorg. Chem.* **1995**, *34*, 6421−6422.

(27) Amouyal, E.; Homsi, A.; Chambron, J.-C.; J.-P., S. *J. Chem. Soc., Dalton Trans.* **1990**, 1841.

(28) Ishow, E.; Gourdon, A.; Launey, J.-P.; Chiorboli, C.; Scandola, F. *Inorg. Chem.* **1999**, *38*, 1504−1510.
(29) Ishow, E.; Gourdon, A.; Launay, J.-P.; Lecante, P.; Verelst, M.; Chiorboli, C.; Scandola, F.; Bignozzi, C.-A. *Inorg. Chem.* **1998**, *37*, 3603−3609.
(30) Campagna, S.; Serroni, S.; Bodige, S.; MacDonnell, F. M. *Inorg. Chem.* **1999**, *38*, 692−701.
(31) Chiorboli, C.; Bignozzi, C. A.; Scandola, F.; Ishow, E.; Gourdon, A.; Launay, J.-P. *Inorg. Chem.* **1999**, *38*, 2402−2410.
(32) Flamigni, L.; Encinas, S.; Barigelletti, F.; MacDonnell, F. M.; Kim, K.-J.; Puntoriero, F.; Campagna, S. *Chem. Commun.* **2000**, 1185−1186.
(33) Bolger, J.; Gourdon, A.; Ishow, E.; Gourdon, A.; Launay, J.-P. *Inorg. Chem.* **1996**, *35*, 2937−2944.
(34) Lincoln, P.; Norden, B. *Chem. Commun.* **1996**, 2145−2146.
(35) Staffilani, M.; Belser, P.; De Cola, L.; Hartl, F. *Eur. J. Inorg. Chem.* **2002**, 335−339.
(36) Lay, P. A.; Sargeson, A. M.; Taube, H. *Inorg. Synth.* **1986**, *24*, 291.
(37) Gritzner, G.; Kůta, J. *Pure Appl. Chem.* **1984**, *56*, 461−466.
(38) Krejčík, M.; Daněk, M.; Hartl, F. *J. Electroanal. Chem.* **1991**, *317*, 179−187.
(39) Kleverlaan, C. J.; Stufkens, D. J.; Clark, I. P.; George, M. W.; Turner, J. J.; Martino, D. M.; van Willigen, H.; Vlček, J. A. *J. Am. Chem. Soc.* **1998**, *120*, 10871.
(40) Vergeer, F. W.; Kleverlaan, C. J.; Stufkens, D. J. *Inorg. Chim. Acta* **2002**, *327*, 126−133.
(41) Nakamaru, K. *Bull. Chem. Soc. Jpn.* **1982**, *55*, 2697.
(42) Balzani, V.; Juris, A.; Venturi, M.; Campagna, S.; Serroni, S. *Chem. Rev.* **1996**, *96*, 759−833.
(43) De Cola, L.; Belser, P. *Coord. Chem. Rev.* **1998**, *177*, 301−346.
(44) Damrauer, N. H.; McCusker, J. K. *J. Phys. Chem. A* **1999**, *103*, 8440−8446.
(45) Albano, G.; Belser, P.; Daul, C. *Inorg. Chem.* **2001**, *40*, 1408−1413.
(46) Fees, J.; Kaim, W.; Moscherosch, M.; Matheis, W.; Klíma, J.; Krejčík, M.; Záliš, S. *Inorg. Chem.* **1993**, *32*, 166−174.
(47) Kober, E. M.; Caspar, J. V.; Sullivan, B. P.; Meyer, T. J. *Inorg. Chem.* **1988**, *27*, 4587−4598.
(48) Creutz, C.; Chou, M.; Netzel, T. L.; Okumura, M.; Sutin, N. *J. Am. Chem. Soc.* **1980**, *102*, 1309−1319.
(49) Kober, E. M.; Caspar, J. V.; Lumpkin, R. S.; Meyer, T. J. *J. Phys. Chem.* **1986**, *90*, 3722−3734.